Planetary and Space Science 189 (2020) 104989

Contents lists available at ScienceDirect

Planetary and Space Science

journal homepage: www.elsevier.com/locate/pss

Planetary Terrestrial Analogues Library project: 1. characterization of samples by near-infrared point spectrometer

C. Lantz [a,*], F. Poulet [a], D. Loizeau [a], L. Riu [b], C. Pilorget [a], J. Carter [a], H. Dypvik [c], F. Rull [d], S.C. Werner [c]

[a] Institut d'Astrophysique Spatiale, CNRS/Université Paris-Saclay, Orsay, France
[b] Institute of Space and Astronautical Science, Sagamihara, Japan
[c] Department of Geosciences, CEED/GEO, University of Oslo, Oslo, Norway
[d] Department of Condensed Matter Physics, Crystallography and Mineralogy, University of Valladolid, Valladolid, Spain

A B S T R A C T

The PTAL project aims at building and exploiting a database involving several analytical techniques, the Planetary Terrestrial Analogues Library, to help characterizing the mineralogical evolution of terrestrial bodies, starting with Mars. A total of 94 natural Earth rocks have been collected from selected locations around the world to get a selection of analogues for Martian geology. The PTAL library gathers a variety of igneous rocks from different plutonic and volcanic origins and compositions, associated to different environments and levels of aqueous alteration. Samples of impact craters and sedimentary units are also present.

The full set of samples will be characterized with optical thin section analysis and XRD (Oslo University, Norway), NIR spectroscopy (Paris-Saclay University, France), Raman spectroscopy (Valladolid University, Spain) and LIBS (Paul Sabatier University, France). The multianalytical study used within the PTAL project provides an unique opportunity to coordinate minerals/elements detection by different techniques that are similar to the instruments onboard current and forthcoming Martian missions. Such combined analysis should give the opportunity to prepare and improve ExoMars/ESA-Roscosmos and Mars2020/NASA observations. This paper focuses only on the NIR measurements and interpretations.

The diversity of the PTAL samples is well revealed by the diversity of spectra from the NIR observations. The detected minerals are representative of various formation, alteration and geochemical environments. The major diagnostic features observed are those of primary Fe^{2+} bearing silicates like olivine or pyroxene with low and/or high calcium content; altered silicates detected with vibrational features associated to OH and/or H_2O and/or metal-OH features; oxides; zeolites; and carbonates.

This collection brings together a set of rocks and minerals that have been reported elsewhere in the Solar System and particularly on Mars.

1. Introduction and context

Near-infrared reflectance (NIR) spectroscopy has long been recognized as very favorable for identifying diagnostic features of rock-forming minerals. Most hydrous and anhydrous silicates, carbonates, sulfates, and other salts can be detected using this technique. Of special interest is the detection of the secondary minerals, which can provide key clues for deciphering the geochemical conditions of their formation and the history of the water-related alteration. This fast, cost-efficient, and nondestructive technique has been greatly developed over the past 20 years for both space exploration and laboratory characterization.

Among space applications, the visible and near-infrared imaging spectrometers OMEGA/Mars Express and CRISM/Mars Reconnaissance Orbiter in the range 1.0–2.6 μm have revealed a high degree of mineralogical diversity on Mars down to sub-kilometer scale (Bibring et al., 2006; Murchie et al., 2009). The detection and the mapping of several classes of aqueous minerals (including phyllosilicates, sulfates, carbonates, hydrated silica) indicate that Mars has likely hosted conditions that allowed liquid water to remain stable over long periods of time (Gendrin et al., 2005; Poulet et al., 2005; Ehlmann et al., 2008; Milliken et al., 2008; Carter et al., 2013a). The widespread occurrence of these altered products and the diversity of settings in which they occur also point to a rich and complex history of water-rock interaction in diverse surface and subsurface environments. These rocks are considered to be among the best targets in which in situ investigations by Mars2020 and ExoMars may discover potential biorelics at microscopic scale (Farmer and des Marais, 1999; Westall et al., 2013).

This very next generation of space missions to Mars will carry for the first time in situ NIR spectroscopy instruments. The NASA Mars2020 rover will benefit from the SuperCam suite of instruments whose infrared spectrometer IRS operates in the range 1.3–2.6 μm with a spatial resolution of a few millimeters at a typical distance of 2–3 m (Wiens et al.,

* Corresponding author.
E-mail address: cateline.lantz@universite-paris-saclay.fr (C. Lantz).

https://doi.org/10.1016/j.pss.2020.104989
Received 21 January 2020; Received in revised form 19 May 2020; Accepted 21 May 2020
Available online 27 May 2020

Table 1
Identities and provenance of PTAL samples analyzed in this paper. See the text in dedicated sections for more details. Lithology informations with a question mark refer to samples « possibly made of ».

Site name/ Rock type	Location	Sample number (lithology)	Section
Dry Valleys	Antarctica	DV16-001 (gabbro)	3.1
Rum	Scotland	RU16-001 (ferropicrite)	3.1
impact rocks	*various locations*	GN16-001, VR16-021 (impact melt); WH16-005, −014 (suevite)	3.2
impact breccias	Brazil	VA16-001, VO16-002 (polymict breccia); VO16-001 (volcanic breccia); VO16-003 (Serra basalt)	3.3
Jaroso Ravine	Spain	JA08-501 (jarosite); −502 (quartz); −503 (fracture fill in gneiss)	3.4
Rio Tinto		RT03-501 (pegmatite w/quartz); −502 (clay sulfates); −503 (pyrite and sulfates?)	3.4
Oslo Rift	Norway	BR16-001, −002, UL16-001 (gabbro)	3.5
Leka Island		LE16-001, −003, −012, (harzburgite), −016 (harzburgite?); −002, −004, −005, −010, −017 (dunite); −006, −007 (chromite); −008 (dunite/ harzburgite); −009, −011, −014 (gabbroic layer); −013 (pillow lava); −015 (serpentine conglomerate)	3.7
several sites	Iceland	IS16-001, −002, −003, −004, −005, −013 (ferropicrite), −015, −016 (ferropicrite?); −006, −007, −008 (tholeiitic lava); −009 (tholeiitic sandstone); −010, −011, −012, −014 (solfatara precipitation)	3.6
John Day Formation	USA	JD16-001 (andisol); −002 (sandstone); −003 (entisol, weathered tuff); 004 (altered basalt); −005, −007 (unaltered basalt); −006 (alfisol, weathered basalt); −008 (alfisol, weathered tuffaceous siltstone); −009 (unweathered siltsone); −010, −012 (oxisol on rhyolite); −011, −013 (rhyolite); −014 to −019 (weathered rhyolite); −020, −021 (weathered alkali olivine basalt); −022 (weathered andesite); −023, −024 (partly weathered andesite)	3.8
Gran Canaria	Canary Islands	AG16-001 (basanite); BT16-001 (sandstone); BT16-002 (hyaloclastite); CB16-001 (pumice/basanite), FA16-001, −002, −003 (altered phonolite); RN16-001 (olivine/pyroxene alkaline lava); TO16-001 (tephriphonolite)	3.9
Tenerife		AD16–001, MR16-002 (phonolite); AM16-001, −002 (sandstone); MR16-001 (basanite); TF16-002, −028, −059, −066 (altered phonolite)	3.9

2016). Onboard the Rosalind Franklin rover of the ESA-Roscosmos ExoMars mission, a point spectrometer will also analyse Mars surface in a similar spectral range (1.15–3.30 μm) and at cm-scale spatial resolution: the Infrared Spectrometer for ExoMars (ISEM) (Korablev et al., 2017). The NIR investigation of the ExoMars mission will be complemented in the subsurface in the range 0.4–2.2 μm with a point spectrometer Ma-MISS hosted directly in the drill (De Sanctis et al., 2017), and in the internal laboratory at grain scale (pixel size of 20 μm) in the range 0.6–3.65 μm with the hyperspectral microscope MicrOmega (Bibring et al., 2017).

Both mission explorations are driven by the search of the ingredients for the planet past/present habitability like hydrated and organic materials. Multiple spectroscopic techniques shall be used to achieve this goal. The ESA and NASA rovers will bring NIR instruments along with Raman spectrometers like RLS (Rull et al., 2017), SHERLOC (Beegle et al., 2017) or the SuperCam remote Raman (Wiens et al., 2017), and an additional LIBS system in the case of Mars2020. It will be crucial to coordinate the results obtained with these different techniques, sensitive to different phases, to point toward the best mineral identification and to maximize the scientific return of future missions.

Aiming to complement existing planetary analogue rock and mineral libraries, the PTAL project (Werner et al., 2018) shall represent a new resource for planetary scientists, namely a Planetary Terrestrial Analogues Library, in order to help the mineralogical characterization of planetary analogues through different techniques, some of which are used in space. The following techniques applied to characterize the samples are distributed over the partners of the PTAL consortium: X-ray Diffraction (XRD) and thin section analysis at Oslo University (Norway), point and imaging spectroscopy in NIR at Paris-Saclay University (France), Raman spectroscopy at Valladolid University (Spain), and Laser Induced Breakdown Spectroscopy (LIBS) at Toulouse University (France). Then spectroscopic data from all these techniques shall feed the PTAL database that will be publicly available by the end of the project (2020), with the ultimate goal of supporting the operations and the analyses of in situ investigations by the future rovers on Mars by assessing results of various instrument combinations.

The IAS team at Paris-Saclay University is in charge of the near-infrared analysis within the PTAL project. Measurements are made with a commercial FTIR (Fourier Transform Infrared) instrument that mimics the spectral characterization of the rover point spectrometers, and with the flight spare model of MicrOmega/ExoMars. In this paper, we will focus on data acquired by the point spectrometer, while spectral analyses obtained from the imaging spectrometer MicrOmega will be presented in a forthcoming publication (Loizeau et al., in prep.).

The core of the PTAL analogue materials suite consisting in 94 powder samples is divided according to their site collection (Table 1). We also give here basic lithology information on the samples. Details on the field campaigns, sample preparation and analysis with XRD and thin sections will be presented in a forthcoming publication (Dypvik et al., in prep.). Note that experimental samples as well as ExoMars landing site analogues were included to be part of the PTAL collection during the project. These additional PTAL samples have been already presented in a separate paper (Viennet et al., 2017) or will be described in a forthcoming paper (Krzesinska et al., in prep.).

After a brief presentation of the methodology (section 2), we present the spectral data and detailed mineralogical features for each sample in section 3. The results are then discussed in the context of the mineralogical properties of landing sites selected for Mars2020 and ExoMars.

2. Method

2.1. Sample preparation

After being collected by the PTAL team (lead by H. Dypvik in close cooperation with local experts), all the 94 terrestrial rock samples were first cleaned and cut for thin section analysis as a first step to provide sufficient information on lithology (Dypvik et al., in prep.). Then, samples were crushed using a sling mill before final crushing in a micronizer. Thus, spectra for XRD, point NIR, Raman and LIBS were acquired on crushed samples (powder with grain size < 100 μm, optically controlled). Working on powders allows to obtain homogeneous sample for which the spatial information provided by the NIR point spectrometer setup is sufficient to characterize the major phases whilst maximizing signal-to-noise through enhanced scattering.

2.2. Measurement procedure

Reflectance spectroscopy in the range 0.8–4.2 μm was performed using a Fourier Transform IR spectrometer (Perkin Elmer Spectrum 100) under ambient temperature and pressure conditions with a spectral resolution of 4 cm^{-1}. The system uses biconical reflectance (the incoming light is projected to an ellipsoid mirror and focused onto the sample, then scattered and the diffuse part is collected by another ellipsoid mirror — the Selector Diffuse Reflectance Accessory by Specac). Each spectrum

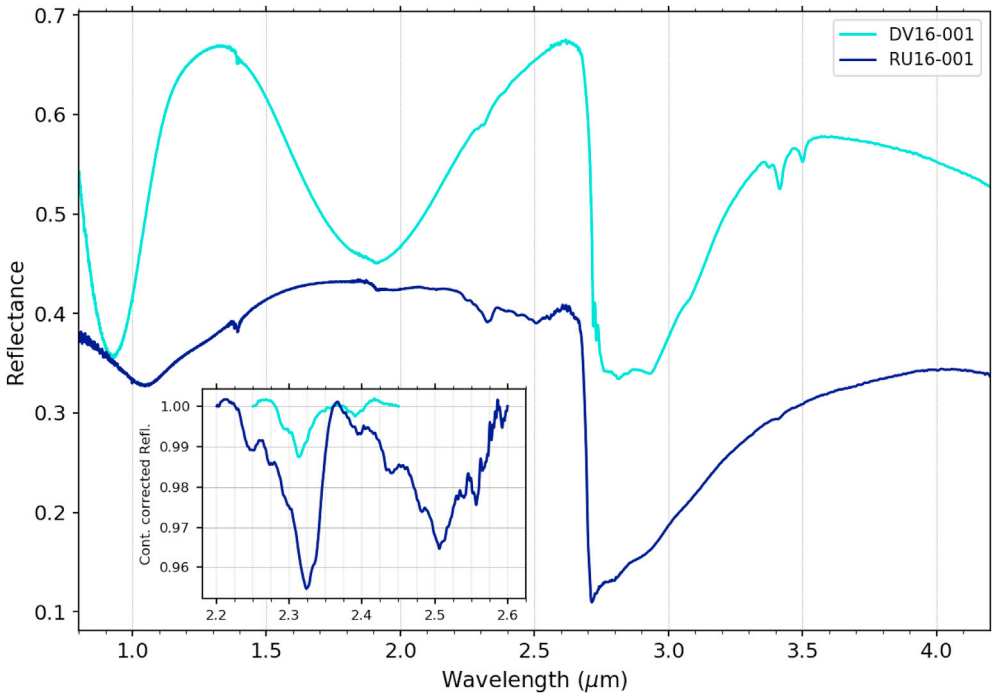

Fig. 1. NIR spectra of samples from Antarctica and Scotland regions. The inset plot shows the continuum corrected spectra in the range 2.2–2.6 μm to highlight the different hydrated phases.

presented in this paper corresponds to the average of 50 scans. To calibrate the sample spectra, they were acquired relative to two calibration targets (an Infragold and a Spectralon 99% from Labsphere) with the same viewing geometry and under the same atmospheric conditions. The Infragold has the advantage of presenting a flat spectrum in the studied range, while the Spectralon 99% was used to determine the level of reflectance (close to a perfect diffuser in the visible). Thus, a combination of both samples is used here for the calibration (we multiply the Infragold by a factor to fit the Spectralon reflectance level below 2 μm). Crushed powder samples were observed by sets of 5–10 samples, and both calibration targets were measured at the beginning and at the end of each session (we averaged the two spectra to better correct slight ambient air changes during the measurements). The exact same protocol is followed for each measurement. The collecting spot size is about 1 mm, which should allow to identify all major constituents of the sample that are mixed thanks to the crushing process.

2.3. Expected spectral features

VIS-IR spectroscopy has demonstrated its powerful capability in the detection and identification of mineral phases through characteristic absorption features related to electronic processes, vibrational stretching and/or bending of characteristic molecular bounds. We describe in the following which mineral groups were expected among PTAL samples and how to identify them.

The primary/igneous minerals are the silicates, identified through broad absorption bands around 1 and 2 μm (called bands 1 and 2) associated to their Fe^{2+} content. These features are attributed to both olivine (band 1) (King and Ridley, 1987) and pyroxene (bands 1 and 2) (Adams, 1974). The precise band positions give hints on the dominating metal within the mineral. We will distinguish the pyroxene end-members LCP (for Low-Calcium Pyroxene with band 2 minimum around 1.9 μm) and HCP (High-Calcium, band around 2.3 μm) (Cloutis and Gaffey, 1991; Sunshine and Pieters, 1993). Olivine can sometimes be hidden behind the pyroxene band 1, and a clear detection within this project PTAL NIR study will rely either on the absence of band 2 or a clear multi-shape of the band 1 as present in single olivine (especially the shoulder a 1.3 μm). A more detailed analysis on the band area ratio could help recognizing the amount of each mineral (Cloutis et al., 1986), but the strong dependence of the olivine band shape and depth on grain size and Fe/Mg ratio makes it difficult to characterize mixtures. This would require spectral modeling which is out of scope of the paper. Iron-bearing glasses can also be detected occasionally (Horgan et al., 2014).

Even though quartz and plagioclase are common minerals on Earth or elsewhere, NIR spectroscopy is not favorable to their detection, because the main band in this spectral range (1.3 μm) is weak and hardly discernible in multiphase mixtures (Nash and Conel, 1974).

Several features are associated to ''water''. A broad rounded band in the range 2.7–3.4 μm is due to adsorbed and/or structurally bound H_2O, while the same band with structures such as a sharp 2.7 μm band is diagnostic of OH stretching in phyllosilicates. The presence of H_2O and OH in the mineral is also detected near 1.9 μm, while a feature near 1.4 μm is related to structurally bound OH- vibrations (Salisbury et al., 1991; Sutter et al., 2007).

The 2.2–2.5 μm range is dominated by additional bands linked to Si-OH and/or metal-OH (Al, Fe, Mg) absorptions. In the first case, a double absorption band centered at 2.21–2.25 μm is detected (Langer and Flörke, 1974). In the second case, the band positions allow to derive cationic mineral composition (Bishop et al., 2002, 2008). Some of these secondary minerals have a sufficient number of bands to give a unique match, while other samples would be classified according to their families. An easy detection among phyllosilicates is serpentine with its numerous absorptions in this range (Calvin and King, 1997).

Zeolites exhibit absorption bands in the 2.1–2.5 μm region overlapping with above mentioned minerals: in this study, we consider a zeolite absorption when a strong reflectance decrease is observed above 2.35 μm (Cloutis et al., 2002).

Sulfate minerals happen to vibrate in the same energy range and occasionally an unambiguous detection is possible due to multiple features in the 1.4–2.5 μm range (Cloutis et al., 2006).

Carbonate features are located around 2.3, 2.5, 3.45 and 3.98 μm (Hunt and Salisbury, 1971). CH stretching bands due to endogenous organics or contamination in the samples can be superimposed on the main 3.45 μm feature (the antisymmetric 3.38 and 3.41 μm and

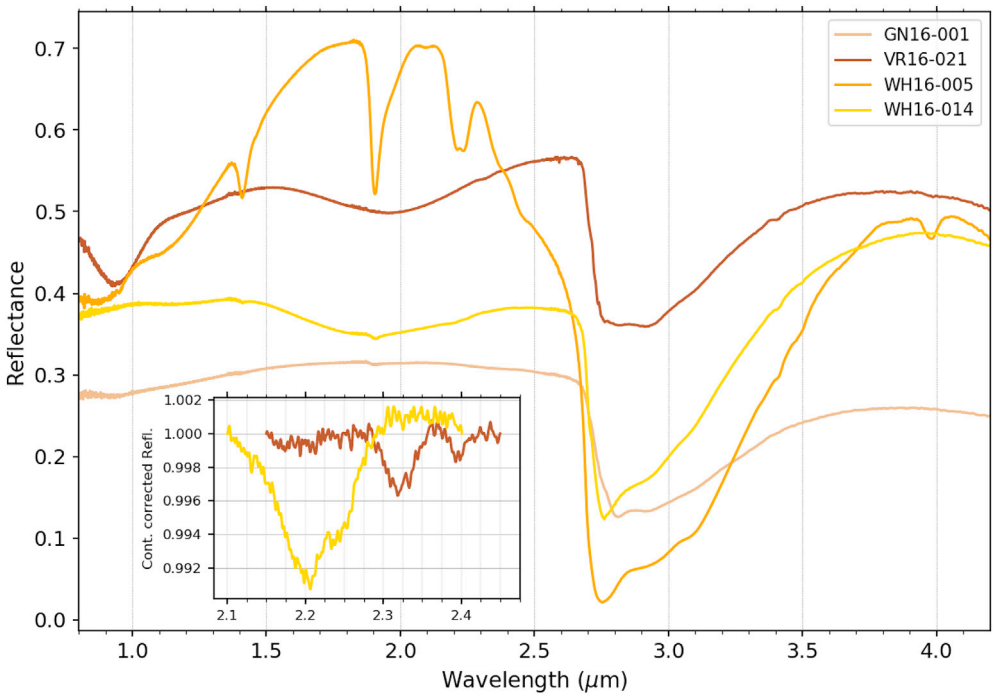

Fig. 2. NIR spectra of impact melt rocks (from three different locations). The inset plot shows the continuum corrected spectra in the range 2.1–2.45 μm to highlight the small hydrated phases in VR16-021 and WH16-014.

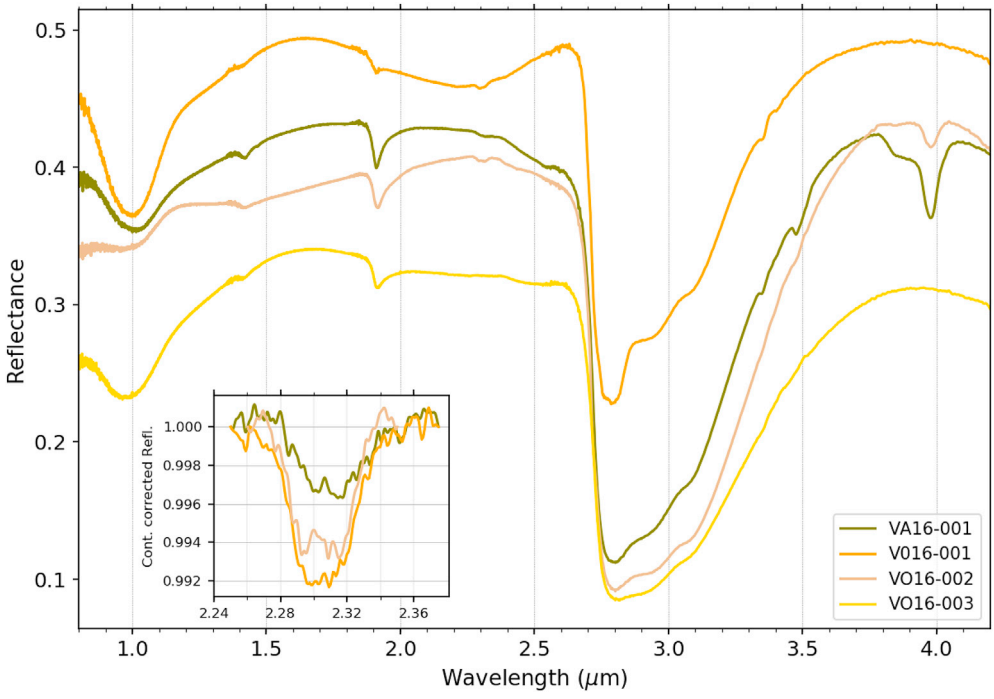

Fig. 3. NIR spectra of impact breccia (from two Brazil sites). The inset plot shows the continuum corrected spectra in the range 2.25–2.38 μm to highlight the small hydrated phases.

symmetric 3.48 and 3.50 μm modes of CH_3 and CH_2 respectively), so that an unambiguous carbonate identification is not possible based only on this detection. Thanks to the extended spectral range of the measurement up to 4.2 μm, the other carbonate feature at ~3.98 μm band can be evaluated, which strengthens the identification of these mineral species.

Another alteration product that we detect here is (hydr)oxide. For example, iron oxide would produce a red slope below 1.8 μm, and/or a shallow absorption around 0.9–1.0 μm. For some specific samples, an hydroxide dominates the spectral signatures (e.g. goethite) (Sherman et al., 1982).

Based on the spectral features that are detected on the PTAL samples, we propose to classify them according to an alteration scheme. End-members of this scale are numbers 1 and 4, associated to samples that are anhydrous and fully altered in a spectroscopic sense respectively. In-between will be samples with traces of hydrated minerals (tiny features on spectrum dominated by primary minerals) as alteration index 2, while

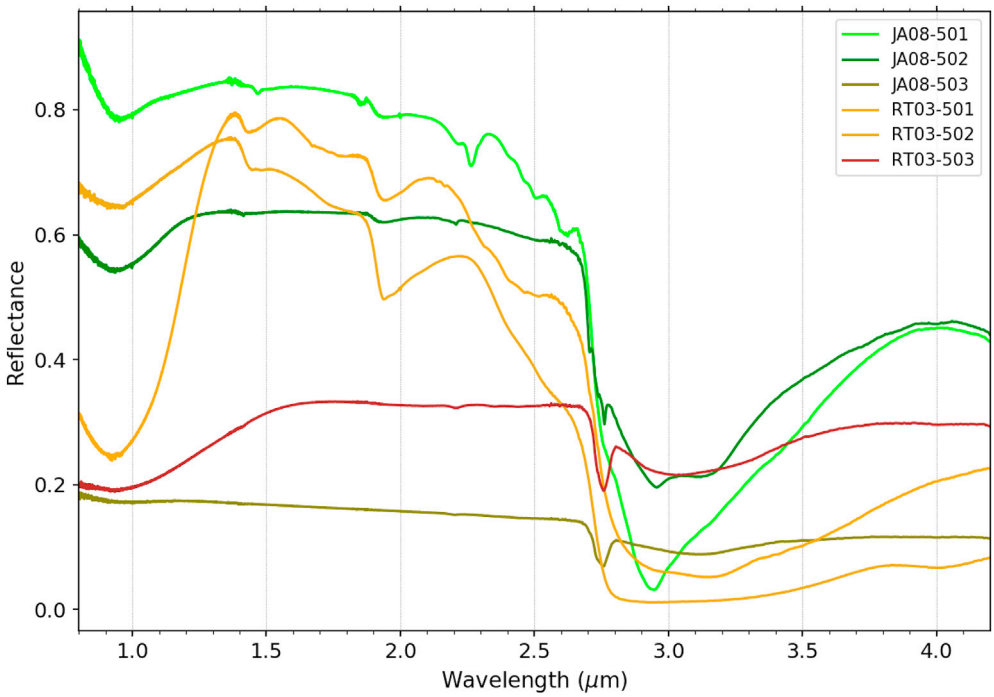

Fig. 4. NIR spectra of Jaroso Ravine and Rio Tinto samples.

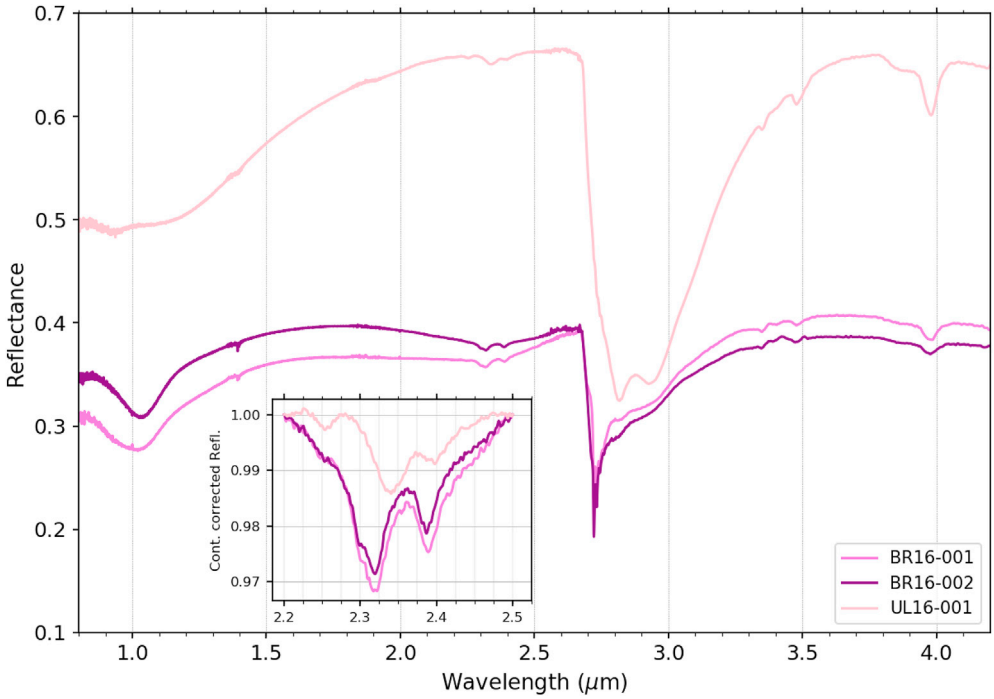

Fig. 5. NIR spectra of Oslo rift samples. The inset plot shows the continuum corrected spectra in the range 2.2–2.5 μm to highlight the different hydrated phases between sample UL16-001 and the samples BR16.

index 3 will refer to samples where both primary and secondary minerals are seen.

3. Results

This section summarizes the detected compounds on each PTAL sample. The spectra are plotted in Figs. 1–15 and the spectral features used for mineral identification are summarized in tabular form (Tables 2–11).

3.1. Antarctica and Scotland samples

Samples DV16-001 and RU16-001 were collected at Dry Valleys, Antarctica (Armstrong 1978) and at Rum, Scotland (Upton et al., 2002) respectively.

The 1 μm band due to pyroxene and/or olivine is prominent in both

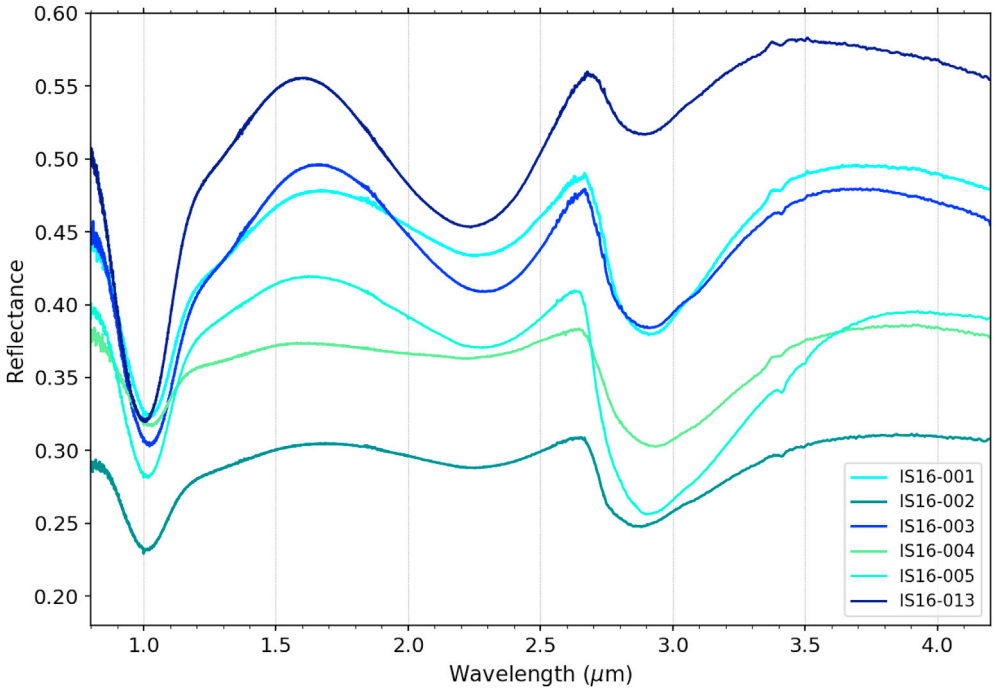

Fig. 6. NIR spectra of Iceland samples — Part 1.

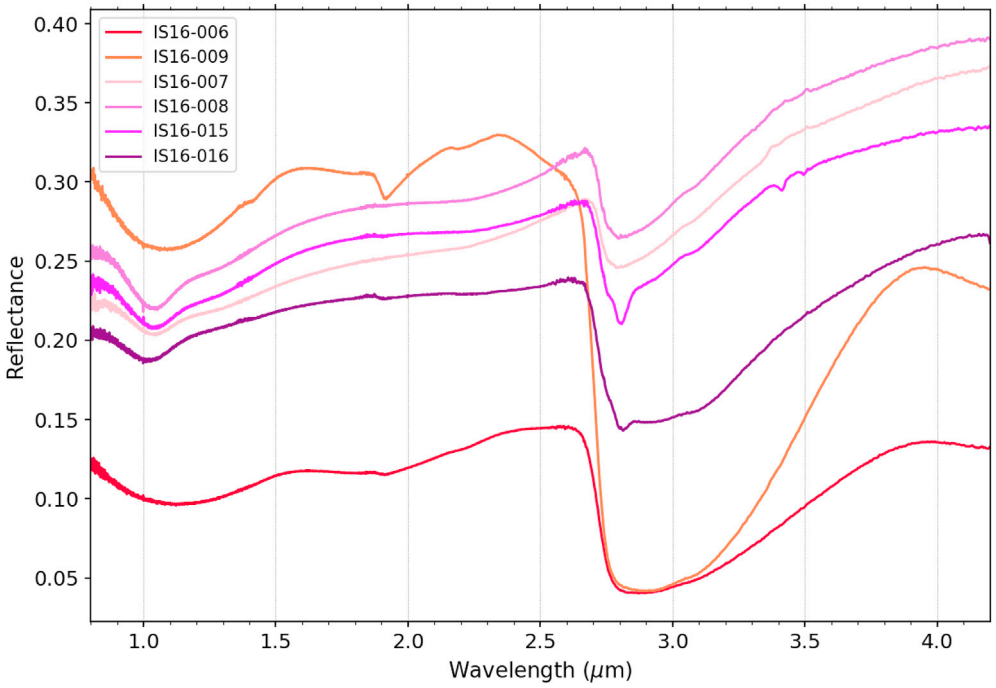

Fig. 7. NIR spectra of Iceland samples — Part 2.

samples with an additional 2 μm pyroxene band for the Antarctica sample. Weak features at 1.4, 1.9 and at ~2.3 μm are indicative of alteration, leading to alteration index of 2. The more prominent alteration feature in the Scotland sample suggests a larger proportion of alteration minerals (index 3), here matching a serpentine spectrum. The alteration product of this last sample is consistent with the primary mineralogy as serpentine is expected to be the primary alteration product of olivine in high temperature conditions. Signatures in both samples around 3.5 μm are attributed to organics, but the origin of these phases is unknown (contamination after collection and/or molecular evidence of biological activity).

3.2. Impact melt rocks

These samples have various origins: GN16-001 was collected in Gardnos, Norway (Kalleson, 2009), VR16-001 in Vredefort, South Africa (Gibson and Reimold, 2008), and WH16-005 and −014 come from Chesapeake Bay, USA (Gohn et al., 2008), in the Eyreville B drill core.

Except for one sample, the spectral features that can be attributed to hydrous minerals are weak, which is consistent with a low degree of

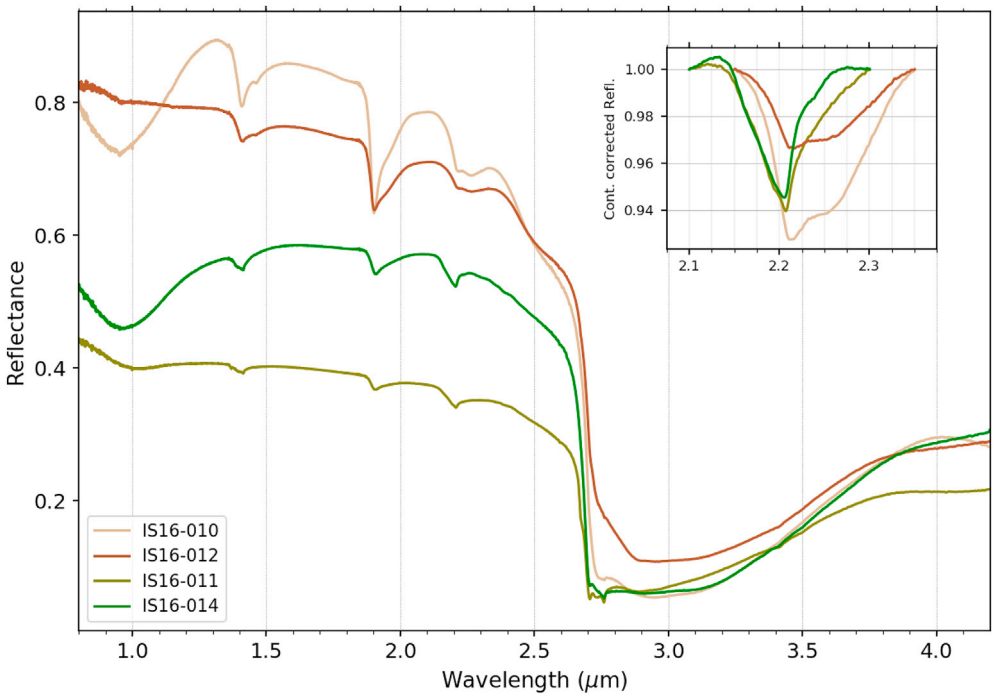

Fig. 8. NIR spectra of Iceland samples — Part 3. The inset plot shows the continuum corrected spectra in the range 2.1–2.35 μm to highlight the different hydrated phases (samples IS16-010 and-012 are alike, the same for −011 and −014).

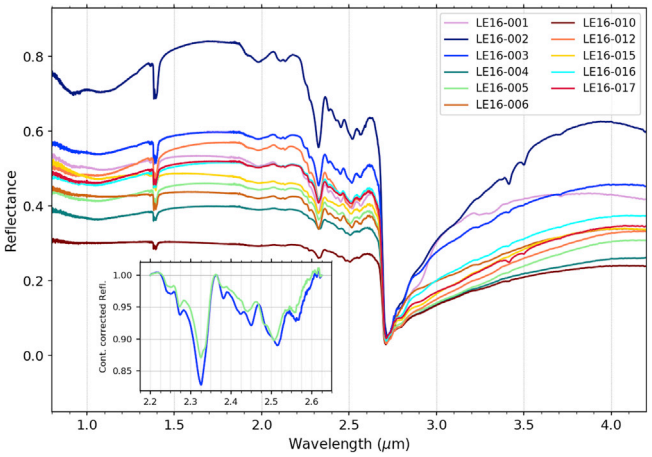

Fig. 9. NIR spectra of Leka samples — Part 1. The inset plot shows the continuum corrected spectra in the range 2.2–2.6 μm to highlight the subtle differences between hydrated phases (serpentine like LE16-003 or 'serpentine + possible other mineral' like LE16-005).

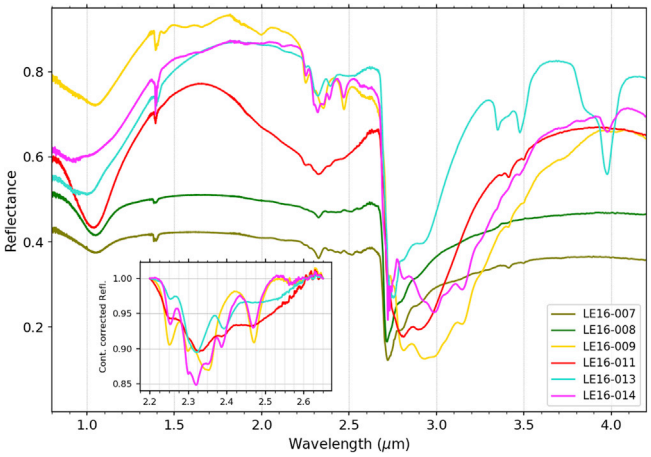

Fig. 10. NIR spectra of Leka samples — Part 2. The inset plot shows the continuum corrected spectra in the range 2.2–2.6 μm to highlight the several hydrated phases in LE16-009, −011, −013, and −014.

alteration. The most distinct sample is the core sample from Chesapeake Bay Crater WH16-005 that shows significant enrichment in hydrous mineral(s) as evidenced by the strong 1.4, 1.9, and 2.20–2.23 μm metal-OH features. We attribute these signatures to a possible illite or micas. Carbonate is also present, possibly diagenetically formed. Surprisingly, the other core sample from the same site shows much less hydration, which could suggest a non-uniform diagenetic alteration at m-scale since only ~10 m separate the two samples.

3.3. Impact breccias in basaltic formations

Sample VA16-001 was collected at Vista Allegre (Crosta et al., 2010) while samples VO16-001 and −002 come from Vargeao Dome (Crosta et al., 2012).

As evidenced by the identification of olivine or pyroxene, primary basaltic composition is still present in the NIR spectra of 3 of 4 of these impact breccias of volcanic rocks. Interestingly, the alteration products (Fe/Mg smectites) are well consistent with a primary basaltic composition. Carbonates are also present, but the origin of this phase is not constrained based on alone NIR characterization of powder samples; it requires a better understanding of the geological setting of the sampling and/or a mapping of the altered phases as performed using the MicrOmega/PTAL setup (Loizeau et al., submitted).

3.4. Jaroso Ravine and Rio Tinto samples

These samples from Spain were collected at Jaroso Ravine (site of jarosite discovery) for JA08-501, −502, and −503 (Martinez-Frias et al., 2004), and at Rio Tinto for RT03-501, −502, and −503

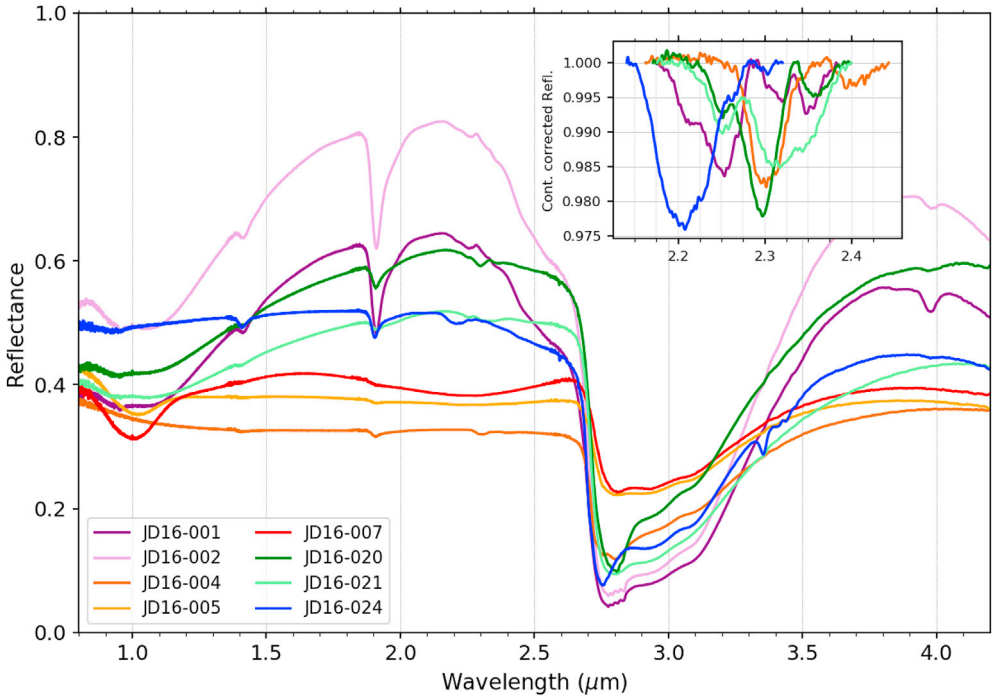

Fig. 11. NIR spectra of John Day Formation samples — Part 1. The inset plot shows the continuum corrected spectra in the range 2.15–2.45 μm to highlight the hydrated phases in JD16-001 (−002 is the same), −004, −020, −021, −024.

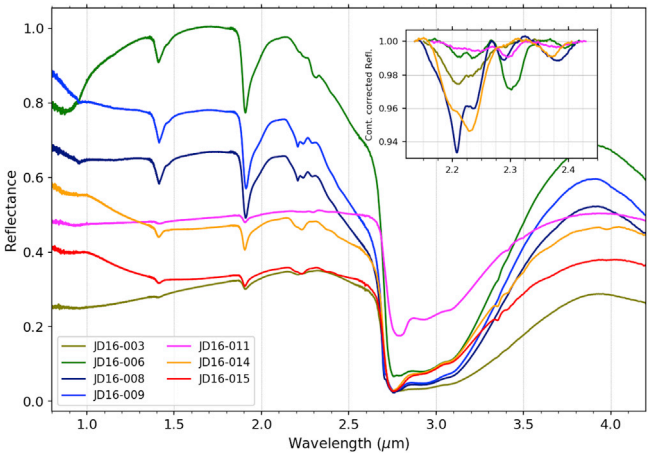

Fig. 12. NIR spectra of John Day Formation samples — Part 2. The inset plot shows the continuum corrected spectra in the range 2.15–2.45 μm to highlight the hydrated phases in JD16-003, −006, −008 (−009 is the same), −011, and −014 (−015 is the same).

(Hudson-Edwards et al., 1999).

The Tinto river and Jaroso Ravine are two fluvial stream systems, with and without permanent water respectively, which have been proposed as potential Earth analogues (Fernandez-Remolar et al., 2004) for the geological and astrobiological exploration of some sulfate-bearing Martian terrains. An important characteristic of the Tinto river is its near constant acidic pH (about 2–3) along its 100 km long course. Rio Tinto is considered a modern model of formation of iron sulfates.

NIR spectra collected in the framework of the PTAL library confirms the identification of jarosite and Fe^{3+}-hydroxides (goethite) as expected. Carbonates have also been identified through weak signatures.

3.5. Oslo rift samples

These samples come from the Norwegian locations of Brattåsen for BR16-001 and −002, and Ullernåsen for UL16-001 (Neumann et al., 1985).

The two BR samples have very similar spectral shape and thus derived-composition, while chlorite is the major secondary product of the UL sample. Strong carbonate signatures are visible in each sample.

3.6. Iceland samples

These samples come from the regions of Haleyabunga (IS16-001, −002, −013), Lagafell (IS16-003, −004, −005), Stapafell (IS16-006, −007, −008, −009), Seltun (IS16-010, −011, −012), Reykjanes (IS16-014), and Vatnsheidi (IS16-015, −016) (Sigmarsson and Steinthorsson 2007).

The mineralogy of these samples can be divided into two groups: unaltered to very weakly altered samples (Haleyabunga, Lagafell, Stapafell, Vatnsheidi) and hydrothermal samples (Seltun, Reykjanes) (Table 7). The identification of primary phases (olivine and pyroxene) for the unaltered group is consistent with their lithology: ferropicrite for Haleyabungaa, Lagafell, and Vatnsheidi, tholeiitic for Stapafell. Note, however, that minor alteration is reported for the tholeiitic pillow of the Stapafell samples (IS16-006 and −009). The altered samples are characterized by the presence of hydrated silica and kaolinite, and the absence of sulfur-rich components that would be expected given their geologic context (solfatara precipitation).

3.7. Leka samples

All these samples come from the Leka Island, Norway (Furnes and Stillman, 1988). The Leka Ophiolite Complex represents a part of the oceanic lithosphere which has been extensively serpentinized at the ocean floor. A wide range of temperatures and different primary minerals were metamorphosed to a variety of secondary minerals.

NIR spectra reveal two large families of samples: most Leka samples show definitive serpentine signatures with variations in strength and

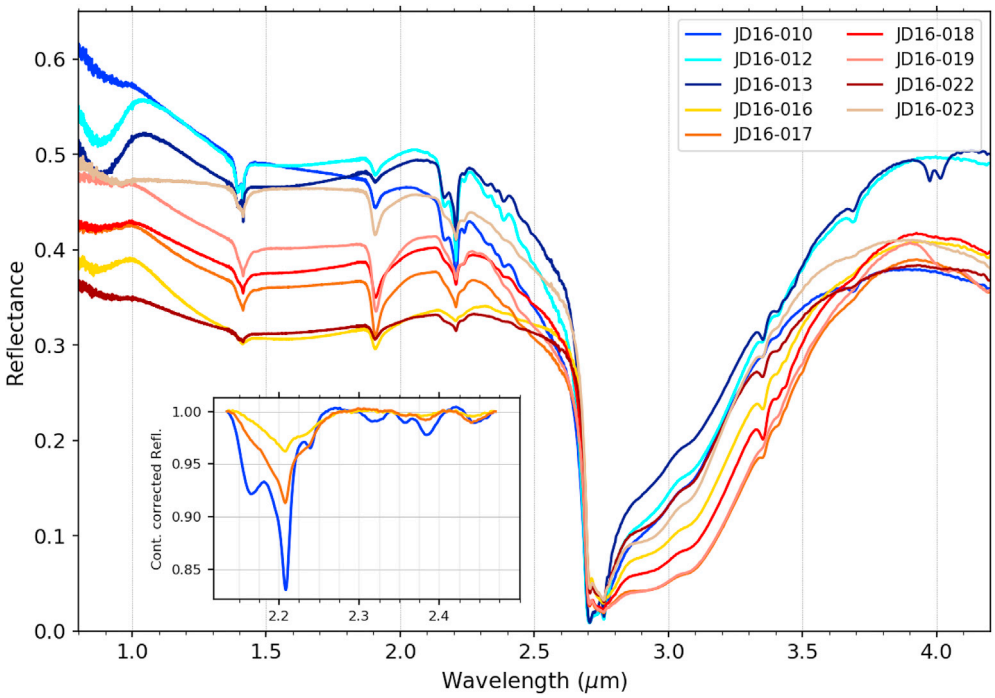

Fig. 13. NIR spectra of John Day Formation samples — Part 3. The inset plot shows the continuum corrected spectra in the range 2.15–2.5 μm to highlight the hydrated phases in JD16-010 (−012 and −013 are the same), −016, and −017 (−018, −019, −022, −023 are the same).

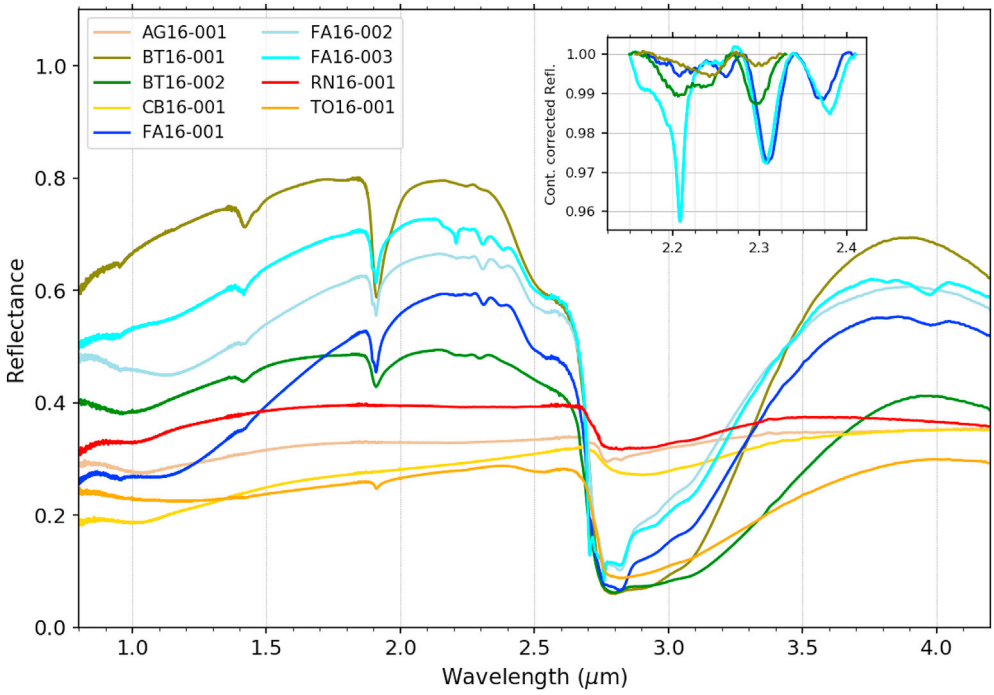

Fig. 14. NIR spectra of Gran Canaria island samples. The inset plot shows the continuum corrected spectra in the range 2.15–2.4 μm to highlight the several hydrated phases in BT16-001, −002, FA16-001 (−002 looks the same), and −003.

only small band shifts (LE16-001 to −008, −010, −012, and −015 to −017), while the other samples show more spectral diversity with the presence of carbonates (except for LE16-011), together with epidote, clinochlore and/or hornblende. The presence of pyroxene (LE16-007, −008 and −011) shows that some samples are not completely altered or formation of secondary pyroxenes (Iyer et al., 2008).

3.8. USA samples

These samples come from the John Day Formation (Oregon), USA (Retallack et al., 2000). They were collected at John Day Valley (JD16-001 to −009), Clarno (−016 to −020), and Painted Hills (the others).

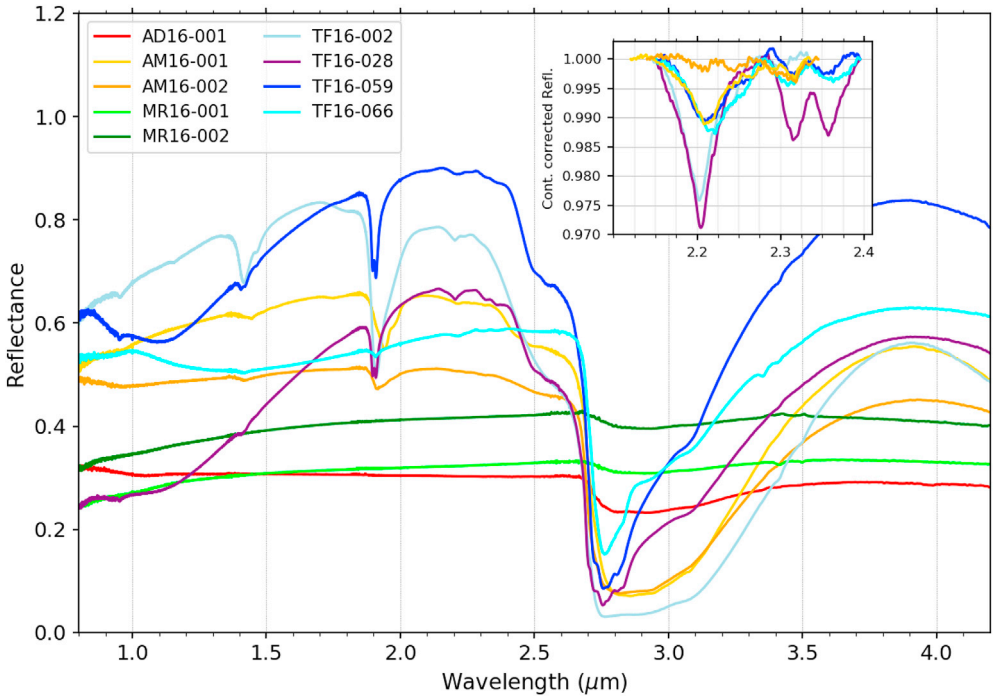

Figure 15. NIR spectra of Tenerife island samples. The inset plot shows the continuum corrected spectra in the range 2.15–2.4 μm to highlight the several hydrated phases in AM16-001, −002, TF16-002, −028, −059 and −066.

Table 2
Mineral features identified in the samples from Antarctica and Scotland regions.

Sample	Alteration Index	Detected compounds and associated features (μm)			
		LCP	Olivine	Serpentine	other hydrated phases
DV16-001	2	0.93, 1.9			consistent with talc/saponite: 1.39, 1.91, 2.29, 2.31, 2.39
RU16-001	3		1.05	1.38 + 1.395, 1.975, 2.11 + 2.135, 2.25, 2.27, 2.325, 2.44, 2.48, 2.51, 2.56	smectite?: 1.91, 2.29, 2.315, 2.39

The mineralogy of these samples as seen by NIR spectroscopy is dominated by phyllosilicates (both smectite-type and/or kaolinite-type) and occasionally mixed with hydrated silica or carbonates. The degree of alteration is however highly variable. The lowest degree of alteration is found for JD16-005 and −007, which is consistent with their lithology recognized as unaltered basalt.

3.9. Canary Islands samples

The samples were picked at the Gran Canaria and Tenerife islands (Troll and Carracedo 2016).

Except for a few samples, the NIR spectral characteristics have numerous water-related features that can be linked to the presence of various hydrated silicates, and sometimes sulfates or hydrated silica. This alteration has likely different origins (surface weathering, hydrothermal activity…) given the various geological settings and lithologies of these samples, and different grades according to the various rock ages in these islands with recent volcanism. Three samples from Gran Canaria (AG16-001, CB16-001 and RN16-001) and three samples from Tenerife (AD16–001 and MR16-001 and −002) show no sign of alteration or very weak alteration signature. Noticeably, many samples from both islands show a variety of signatures linked to the metal-OH bond in the 2.2–2.4 μm domain, together with sharp absorption bands around 1.4 and 1.9 μm, showing the likely presence of a variety of phyllosilicates, a sign of

Table 3
Mineral features identified in the impact melt rocks. * (Ehlmann et al., 2009).

Sample	Alteration Index	Detected compounds and associated features (μm)							
		Pyroxene (LCP ≫ HCP)	Amphibole (Hornblende)	Illite (1M)* or mica	Si—OH	Carbonate	oxide (Fe)	traces of hydrated phases	Unidentified
GN16-001	2						0.93	1.4, 1.9, shape of 2.7	
VR16-021	2	0.94, 1.97	2.32, 2.395						
WH16-005	4			1.41, 1.905, 2.1, 2.21, 2.235, 2.365, 2.45		3.98	shoulder before 1 + red slope		
WH16-014	2				2.25			Al-OH:1.41, 1.91, 2.2	Broad symmetric structure centered at 1.9

Table 4
Mineral features identified in the impact breccias.

Sample	Alteration Index	Detected compounds and associated features (μm)							
		Olivine	Pyroxene (HCP>)	Fe, Mg smectite	Si—OH	Carbonate	oxide (Fe)	traces of hydrated phases	Unidentified
VA16-001	3	1.02		1.42, 1.91, 2.31, 2.54		3.35 + 3.48, 3.85 + 3.98	?: band enlargement at 0.95		
VO16-001	2		1.00, 2.22	1.42, 1.91, 2.30					
VO16-002	4			1.42, 1.91, 2.29 + 2.31		3.85 + 3.98	Shoulder at 0.95		
VO16-003	2		0.97, 2.15		tiny 2.25		?: band enlargement at 0.95	1.42, 1.91	shallow rounded band at 2.5

Table 5
Mineral features identified in the samples from Jaroso Ravine and Rio Tinto sites.

Sample	Alteration Index	Detected compounds and associated features (μm)					
		Jarosite	Goethite	Fe-oxide (goethite type) richer in H_2O or Fe-sulfate (copiapite?)	Oxide (Fe)	Carbonate	traces of hydrated phase
JA08-501	4	whole spectrum					
JA08-502	4		0.93, 1.92			3.98	1.42, 2.21
JA08-503	4				structure below 1.2		1.4, 2.2, 2.75
RT03-501	4		whole spectrum				
RT03-502	4			whole spectrum			
RT03-503	4				structure below 1.5	4.0	illite, lost water?:1.42, 2.21, 2.35, 2.44; 2.75

Table 6
Mineral features identified in the samples from Oslo rift.

Sample	Alteration Index	Detected compounds and associated features (μm)						
		Olivine	HCP	amphibole (Hornblende/ actinolite?)	Chlorite	Carbonate	Oxide (Fe)	Unidentified
BR16-001	3	1.02 + 1.3	1.02, 2.3	2.3, 2.32, 2.39		3.98	?: band enlargement at 0.95	
BR16-002	3		1.04, 2.3	2.3, 2.32, 2.39		3.98		
UL16-001	4				1.4, 1.92, 2.25, 2.34, 2.4, 2.82, 2.93	3.85 + 3.98	red slope below 1.8	0.93

low-temperature alteration of the volcanic rocks. However, the accurate identification of the altered phases is sometimes difficult. A comparison with other PTAL techniques shall be therefore useful for understanding the texture and distribution of alteration products and variations in fluid chemistry.

4. Discussion

4.1. PTAL sample mineralogy as Martian analogue

In this study, we examined the mineralogy of the PTAL samples derived from NIR reflectance spectroscopy. Distinctive assemblages of primary minerals and altered products are identified and point to various modes of aqueous alteration analogue to Mars' past aqueous environments. From this characterization, a scale associated to the degree of alteration (see second column in all tables) for each sample is derived from 1 (only anhydrous minerals) to 4 (fully altered). As discussed below, the diverse NIR mineralogy of the PTAL samples covers different types of Martian alteration settings and conditions recognized in Noachian and Hesperian terrains.

In section 3.1, the samples from Antarctica and Scotland are perfect examples of alteration index 2 (sample DV) whose spectra are dominated by pyroxene with weak hydrated features and alteration index 3 (sample RU) where both olivine and altered minerals are seen. Primary minerals exhibiting a low degree of alteration are common on Mars, including some terrains in the emblematic Nilo-Syrtis region (Mustard et al., 2007).

Samples presented in sections 3.2 and 3.3 originate from impact craters, which are also numerous on Mars. Large impact craters on Mars are recognized as major targets in Martian exploration since they can penetrate potential deep aquifers and create deep radial and concentric faults that can serve as fluid conduits, forming deposits on crater rims, central uplifts and on crater floors (Schwenzer and Kring, 2013; Carrozzo et al., 2017). They also excavated Martian crust providing an unique way to sample the Martian upper crust (e.g. Ehlmann et al., 2011; Bultel et al., 2015) and models show that in the presence of ice in the crust, crater formation can also trigger long lasting hydrothermal systems at or near the surface of the crater floor (e.g. Rathbun and Squyres, 2002). The PTAL melt rocks and suevites from central parts of the different impact craters present different compositions and degrees of alteration. These are probably due to the original target rock mineralogy, the impactor size and composition, along with varying degrees of post-impact changes. From a lithological point of view, these samples might be poorly

Table 7
Mineral features identified in the samples from Iceland.

Sample	Alteration Index	Detected compounds and associated features (μm)						
		Olivine	Pyroxene (HCP > LCP)	Glass	Si-OH	traces of hydrated phase	Kaolin-group	Oxide (Fe)
IS16-001	1	1.025 + 1.30	1.025, 2.275					
IS16-002	1	?	1.01, 2.29			2.75		
IS16-003	1	1.025 + 1.30	1.025, 2.285					
IS16-004	1	1.025 + 1.30	1.025, 2.23					
IS16-005	1	?	1.015, 2.26					
IS16-006	2			1.1, 2.0	1.9, broad 2.2	2.75		
IS16-007	1	1.04 + 1.30	1.04, 2.24			2.75		
IS16-008	1	1.04 + 1.30	1.04, 2.24			2.75		
IS16-009	2			1.1, 2.0	1.4, 1.9, broad 2.2	2.75		
IS16-010	4				Hyalite: 0.95, 1.15, 1.41 + 1.465, 1.8, 1.9+wing, 2.21–2.26, 2.5			Broad 0.95
IS16-011	4	Fe2+ phase: 1.02					1.37, 1.41, 1.91, 2.21, tiny 2.39, 2.71, 2.76	
IS16-012	4				Hyalite: *same as -010*			
IS16-013	1	1.0 + 1.3	1.0, 2.23					
IS16-014	4						*same as -011*	0.96
IS16-015	2	1.045 + 1.30	1.045, 2.25			1.9, 2.8		
IS16-016	2		1.025, 2.25		1.9, 2.2, 2.8			

representative of the central peaks of Martian craters. Actually, their NIR-derived mineralogy significantly differs from the mineralogy of the Martian crater central peaks largely dominated by Fe/Mg clays and hydrated silica (Sun and Milliken, 2015).

Breccia rocks have been identified on Mars but these rocks are too small for the capability of the orbital imaging spectrometers OMEGA and CRISM. Compositional information on Martian breccia comes from the meteorite "BlackBeauty" (NWA8171) and its pairings that are pieces of a polymict regolith breccia with a basaltic composition (Agee et al., 2013; Humayun et al., 2013).

Section 3.4 presents samples from Jaroso Ravine and Rio Tinto with complex assemblage of hydrated sulfates, Fe^{3+} hydroxides and carbonates. These secondary "ferric sulfates" phases are similar to those observed in the Martian sulfate-bearing deposits in Meridiani Planum from in situ observations (Klingelhöfer et al., 2004) and orbital observations (Poulet et al., 2008b; Wiseman et al., 2010; Flahaut et al., 2015).

The implications of the samples present in section 3.5 are not obvious due to the geological context corresponding to a rift feature. On the other hand, the spectra can be used in order to allow better identification of specific minerals and/or types of chlorite-like and hornblende-like mineralogy on Mars.

Unaltered samples, as seen by NIR, from Iceland presented in section 3.6 are analogues of primary unaltered ferropicritic and tholeiitic lithologies, while the altered group is well representative of amorphous silica-rich outcrops, which have been proposed to have formed under acid-steam heated alteration on Mars (Flahaut et al., 2019) (from in situ observation by the Mars Exploration Rover Spirit (Squyres et al., 2008)).

Serpentinized samples from Leka island (Norway) listed in section 3.7 are analogues to deep crust alteration of olivine-rich rocks on Mars. The Leka rocks are the result of the alteration of ancient ocean crust, uplifted ~500 Ma ago (Dunning and Pedersen, 1988). Serpentine has been detected on Mars linked to crater structures and olivine-rich units (Ehlmann et al., 2010; Bultel et al., 2015; Michalski et al., 2019), and in the Martian meteorite Lafayette (Hicks et al., 2014). Bultel et al., (2015) report the presence of serpentine, carbonate and chlorite associated to the same craters. Alteration at moderate temperature (50–350 °C) with hydrous CO_2-rich fluids, of a protolith with mafic to ultramafic composition (moderate to low Si content) can explain serpentinization and carbonation of the rocks and the presence of chlorite. Results from the NIR analysis of the PTAL Leka rocks show similar minerals (serpentine to chlorite/carbonate assemblage) that could be good analogues to the deep alteration observed on Mars. Similar minerals have also been observed in the Nili Fossae region (Ehlmann et al., 2010) near the selected landing site for the Mars2020 mission, discussed in section 4.2.

The extensive clay mineral-bearing deposits on Mars are not consistent with either hydrothermal alteration or subaqueous deposition but rather with aqueous alteration at the surface (Poulet et al., 2009a; Carter et al., 2015). Some of these deposits are morphologically and mineralogically consistent with terrestrial paleosol sequences, and it has been specifically proposed that the John Day paleosol sequence (Oregon) could be an excellent terrestrial analogue to these terrains (Horgan and Christensen 2013). The mineralogy of the PTAL samples collected in the USA settings presented in section 3.8 confirms that the mineralogy of these terrains exhibits a complex assemblage dominated by phyllosilicates locally mixed with hydrated silica, zeolites and carbonates, similar to what has been reported from orbit. The transition from smectites, to kaolinites, to poorly-crystalline phases and zeolites (all observed in PTAL samples) could reflect climatic shift, or may be the result of difference in protolith (kinetics and amount of Si available). Of special interest is the presence of carbonates (Table 9) that has been recently suggested in weathering profiles in Mawrth Vallis (Bultel et al., 2019). Therefore, the PTAL samples could be used to interpret geochemical processes that occurred during the formation of these extensive clay-bearing deposits.

Volcanic activity in the Canary Islands started ~20 Ma years ago

Table 8
Mineral features identified in the samples from Leka. * (Carter et al., 2013b).

Sample	Alteration Index	Detected compounds and associated features (μm)							
		HCP	Serpentine (+possible other mineral)	Carbonate	Epidote*	Chlorite	Hornblende	Unidentified	Oxide (Fe)
LE16-001	4		1.285, 1.365,1.385 + 1.395, 1.915, 1.98, 2.09 + 2.11, 2.135, 2.25, 2.275, 2.325, 2.38, 2.425, 2.45, 2.49 + 2.515, 2.57, 2.723					structure 0.95–1.07, 3.25 + 3.32, 3.7	
LE16-002	4		*same as -001*					structure 0.92–1.1, 3.7	red slope below 1.8
LE16-003	4		*same as -001 but* 2.715					*same as -001 but 0*.94–1.06	
LE16-004	4		1.385 + 1.395, 1.98, 2.09 + 2.11, 2.135, 2.25, 2.275, 2.325 (+kaolinite?: +2.335, 2.375, 2.40, 2.44, 2.48, 2.505, 2.56)						
LE16-005	4		1.285, 1.365,1.385 + 1.395, 1.98, 2.09 + 2.11, 2.135, 2.25, 2.275, 2.325 (+kaolinite?: +2.335, 2.375, 2.445, 2.48, 2.505, 2.56, 2.71)						
LE16-006	4		*same as -001* + 2.71-2.72					3.7	
LE16-007	3	1.05, 2.3	*same as -001 but* no 1.365					3.7	
LE16-008	3	1.05, 2.3	1.38 + 1.395, 1.98, 2.10, 2.135, 2.25, 2.275, 2.325, 2.385, 2.425, 2.45, 2.49 + 2.52, 2.57, 2.715						
LE16-009	4			4.03	1.445, 1.56, 1.66, 2.25, 2.355, 2.47, 3, 3.05, 3.15	Mg-rich: 1.395 + 1.405, 2.0, 2.12, 2.25, 2.3, 2.575, 2.723, 2.75, 3, 3.05, 3.15		3.73	
LE16-010	4		1.285, 1.38 + 1.395, 1.915 + 1.98, 2.09 + 2.11, 2.135, 2.25, 2.275, 2.325 + 2.335, 2.385 + 2.4, 2.435 + 2.44+2.45, 2.48 + 2.505, 2.56, 2.715						
LE16-011	3	1.03, 2.3				clinochlore: 1.392 + 1.398, 1.9, 2.25, 2.325, 2.47, 2.8, 2.9	2.3, 2.39, 2.72, 2.73		
LE16-012	4		1.285, 1.365,1.38 + 1.395, 1.915, 1.98, 2.09 + 2.11, 2.135, 2.25, 2.275, 2.325, 2.385, 2.45, 2.48 + 2.51, 2.56, 2.715					Structure 0.92–1.1	
LE16-013	4			3.35 + 3.415, 3.48, 3.85 + 3.975		1.392 + 1.398+1.405, 1.9–2, 2.12, 2.25, 2.32, 2.8, 2.9	2.39, 2.54, 2.72, 2.73, 2.745, 2.76		
LE16-014	4			3.35, 3.48, 3.98	1.445, 1.56, 1.66, 2.25, 2.355, 2.47, 3, 3.05, 3.15	1.392 + 1.398+1.405, 1.9–2, 2.12, 2.25, 2.3, 2.32, 2.8, 2.9	2.3, 2.39, 2.72, 2.73, 2.745, 2.755	3.74, 3.85	
LE16-015	4		*same as -010*						
LE16-016	4		*same as -012*					Structure 0.92–1.1; 3.7	
LE16-017	4		*same as -012*					Structure 0.92–1.1; 3.7	

(Schmincke, 1982). The ongoing volcanic activity and the humid to arid environments of the islands have created a large variety of alteration environments on various primary rocks (basaltic lava flows to ash deposits) from slow surface weathering to hydrothermal alteration. Surface alteration of basaltic rocks has been shown to be widespread on Mars (e.g. Carter et al., 2013a; Carter et al., 2015) but hydrothermal alteration has been discussed extensively and possibly identified from the surface at the Columbia Hills by the Spirit rover (e.g. Squyres et al., 2008). This set of samples (section 3.9) with different stages of alteration in different contexts could help better constraining the alteration history of various regions of Mars.

4.2. PTAL sample mineralogy as analogue to the forthcoming landing sites

The Mars2020/NASA mission will land in Jezero crater and plans to drive up to the highlands west of the crater. The bright floor unit and paleo delta/fan deposits show the presence of both olivine and carbonates with apparent varying amounts, and the presence of Fe/Mg-smectites in some outcrops. Similar minerals have been mapped outside of the crater, in the watershed that fed the paleo-lake that once filled Jezero crater (Goudge et al., 2015). Hydrated minerals identified inside Jezero crater were likely formed mainly in the rocks of the watershed and transported into the crater by the fluvial activity, although

Table 9
Mineral features identified in the samples from the John Day Formation.

Sample	Alteration Index	Detected compounds and associated features (μm)										
		Olivine	HCP	Smectite	Kaolinite	Other phyllosilicates	Si-OH	Traces of hydrated phase	Zeolite	Carbonate	Oxide (Fe)	Unidentified
JD16-001	4					Mica (celadonite/biotite?): 0.95, 1.415, 1.91, 2.21 + 2.25, 2.32, 2.35			?: 2.45 + 2.55	3.85, 3.98		
JD16-002	4					*same as -001*			*same as -001*	3.98		
JD16-003	2						1.41, 1.91, 2.21-2.24					
JD16-004	2			Fe/Mg: 1.41, 1.91, 2.31, 2.41								
JD16-005	2		1.03, 2.28					minor: 1.41, 1.91, 2.22, 2.31, 2.43				
JD16-006	4			Fe/Mg: 1.41 + 1.47, 1.91, 2.3, 2.39			2.21-2.24					
JD16-007	2	1.0 + 1.3	1.0, 2.28					1.9				
JD16-008	4			Al/Fe/Mg: 0.95, 1.41 + 1.47, 1.91+wing, 2.21, 2.24, 2.29, 2.38								
JD16-009	4			*same as -008*								
JD16-010	4				1.395 + 1415, 1.9, 2.16 + 2.21, 2.24, 2.32, 2.36, 2.39						0.9	Broad symmetric structure centered at 1.6; 3.7
JD16-011	2	Fe2+phase?: structure 1.1		Fe/Mg nontronite/saponite: 1.42, 1.91+wing, 2.295, 2.38			2.2–2.25					
JD16-012	4				*same as -010*						*same as -010*	*same as -010*
JD16-013	4				*same as -010*					3.355, 3.41, 3.475, 3.975, 4.015	*same as -010*	*same as -010*
JD16-014	3			Fe/Mg nontronite/saponite: 1.42, 1.91+wing, 2.37		2.19-2.23				3.98	0.9	Broad symmetric structure centered at 1.6
JD16-015	3			*same as -014*		*same as -014*					*same as -014*	*same as -014*
JD16-016	3			wing 0.96, 1.415, 1.91+wing, 2.21, 2.24, 2.38, 2.44							0.9	*same as -014*
JD16-017	4			kaolinite + smectite: wing 0.96, 1.39 + 1.415,							0.9	*same as -014*

(*continued on next page*)

Table 9 (*continued*)

Sample	Alteration Index	Detected compounds and associated features (μm)										
		Olivine	HCP	Smectite	Kaolinite	Other phyllosilicates	Si-OH	Traces of hydrated phase	Zeolite	Carbonate	Oxide (Fe)	Unidentified
				1.91+wing, 2.16, 2.21, 2.24, 2.38, 2.44								
JD16-018	4			*same as -017*						3.36, 3.41, 3.44, 3.98 + 4.03	0.9	*same as -014*
JD16-019	4			*same as -017*						3.35, 3.41, 3.50, 4.03		*same as -014*
JD16-020	4			Fe/Mg: 0.96, 1.41, 1.91, 2.30, 2.36			2.21-2.25			3.98		
JD16-021	4					chlorite (clinochlore?): 1.4, 1.91+wing, 2.25, 2.31 + 2.35,						
JD16-022	3			*same as -017*							0.9	*same as -010*
JD16-023	4			*same as -017*								
JD16-024	3			Al: 0.96, 1.41, 1.9, 2.21 + 2.23, 2.27, 2.3						3.355, 3.41, 3.44, 3.98		

Table 10
Mineral features identified in the samples from the Gran Canaria island.

Sample	Alteration Index	Detected compounds and associated features (μm)							
		Olivine	HCP > LCP	Chlorite	Other hydrated silicates	Si-OH	Traces of hydrated phase	Zeolite	Carbonate
AG16-001	1	1.04 + 1.30	1.04, 2.25				2.78, 2.83		
BT16-001	4				Fe/Mg-OH: 2.3	2.25		analcime: 0.96, 1.16, 1.42, 1.78, 1.92, 2.5	
BT16-002	4				Fe/Mg smectite: 0.96, 1.415, 1.91, 2.2, 2.25, 2.3	2.2–2.25			
CB16-001	1	1.02 + 1.3	1.02, 2.2						
FA16-001	4			slope below 2.2, 2.26, 2.375	Al/Fe/Mg-OH: 0.95, 1.42, 1.895 + 1.91, 2.2, 2.31			?: 2.49, 2.54	3.82, 3.98
FA16-002	4			*same as FA16-001*	*same as FA16-001*			*same as FA16-001*	
FA16-003	4			*same as FA16-001*	*same as FA16-001* + kaolin-group: 2.16, 2.2			*same as FA16-001*	*same as FA16-001*
RN16-001	1		1.025, 2.3				2.83		
TO16-001	2				Unidentified: 1.42, 1.91, 2.23, 2.53, 2.76				

some alteration was possible in situ (Goudge et al., 2015). The Fe/Mg-smectites are interpreted to have formed first by aqueous alteration at the surface and subsurface of the regional crust. After the formation of Jezero crater, an olivine unit was emplaced at or near the surface, that was then altered to form Mg-rich carbonates, possibly by serpentinization, as serpentine has also been reported in the region (Ehlmann et al., 2009).

PTAL samples from the Ophiolite complex of the Leka island (Norway) have undergone near complete serpentinization, and some of them show the strong presence of carbonates; the sample from Rum (Scotland) contains serpentine, but olivine is still present, showing a different level of serpentinization. The analysis of these samples could help us better constrain the observations in Jezero crater and surrounding region both from the orbit and at the surface with the future rover.

The ExoMars/ESA-Roscosmos mission will land in Oxia Planum on an extensive, spectrally homogeneous, Fe/Mg-phyllosilicate bearing unit (Quantin-Nataf et al., 2019). Spectra show similarities with Fe/Mg-smectites (saponite type) or other clay minerals (e.g. vermiculite) (Carter et al., 2016; Dugdale et al., 2020). More mineral variability is reported on the Eastern part of the landing site, within and around delta-fan deposits, where signatures of Fe^{2+} smectites have possibly been found, as well as Al-phyllosilicate outcrops and a larger hydrated silica (opal?) stratum (Carter et al., 2016; Quantin-Nataf et al., submitted).

Various PTAL samples show spectra similar to Fe/Mg-phyllosilicates, although a perfect match has not been found yet with the Oxia Planum spectra. MicrOmega observations of the same set of samples might provide additional mineral species present in minor amounts in the samples, and may detect spectra more similar to the Fe/Mg-phyllosilicates of Oxia Planum (Loizeau et al., in prep.). Also, analysis of upcoming samples from alteration experiments in the PTAL project may lead to a better

Table 11
Mineral features identified in the samples from the Tenerife island. The inset plot shows the continuum corrected spectra in the range 2.2–2.6 μm to highlight the several hydrated phases in LE16-009, −011, −013, and −014.

Sample	Alteration Index	Detected compounds and associated features (μm)				
		Various phases	Sulfate	Various hydrated silicates	Oxide (Fe)	Carbonate
AD16-001	2	Fe2+: 1.05				3.98
AM16-001	4		Gypsum: 0.97, 1.41 + 1.44+1.49, 1.75, 1.94+shoulder, 2.21, 2.315, 2.45, 2.5			
AM16-002	3			Al/Fe-OH: 0.96, 1.42, 1.91, 2.315, 2.2-2.25		
MR16-001	1	*No detection*				
MR16-002	1	*No detection*				
TF16-002	4			Al-OH (beidelite?): 0.96, 1.15, 1.415 + 1.465, 1.785, 1.91, 2.2, 2.24, 2.3		
TF16-028	4			Unidentified: 0.96, 1.405, 1.9, 1.91, 2.205, 2.315, 2.355, 2.5, 2.55	slope below 2.1	
TF16-059	4			Unidentified: 1.405, 1.42, 1.46, 1.9, 1.91, 2.11, 2.21, 2.315, 2.355, 2.5, 2.55	slope below 2.1	
TF16-066	2	Glass?: broad structure 1.1–2.2		Unidentified: 1.415, 1.91, 2.22, 2.31, 2.365, 2.48		

understanding of the possible formation process of this type of phyllosilicate on Mars (Krzesińska et al., 2019) and how we observe them in the NIR. Some hydrated silica present in the PTAL rock collection (e.g. JD16-003) are likely linked to surface aqueous weathering, as expected for Oxia (Carter et al., 2016).

4.3. Future synergy between PTAL techniques

Some mineral families were not detected during this study because they are largely featureless in the IR range (feldspar, quartz, or high-temperature SiO_2 polymorphs). Thus, one needs to look at XRD (Dypvik et al., in prep) or Raman (Veneranda et al., 2019) data to detect such phases. However, it has been possible to retrieve abundances of these featureless phases along with NIR sensitive minerals on Mars surface remote study thanks to spectral modeling (Poulet et al., 2009b). A follow-up on this study could be to reproduce the PTAL sample NIR spectra and compare to results obtained by the other techniques during the project.

If our analyses confirm that NIR spectroscopy is a powerful technique to reveal the presence of aqueous alteration in the samples, the precise and accurate identification of altered products is sometimes ambiguous, requiring additional and complementary information from other techniques. Coordinated analyses are on-going, revealing pros and cons for each technique (the outcome of these analyses for typical and specific samples is foreseen to be submitted before the end of the PTAL project). Raman results are already available (Veneranda et al., 2019) and LIBS analysis is ongoing. Coordinated analysis between the four spectroscopic techniques, together with thin section data, will be therefore performed.

Another interesting comparison will be made between this study at macroscopic scale on homogeneous samples and the MicrOmega acquisitions at microscopic scale on bulks (Loizeau et al., in prep.).

New samples, specifically chosen to match Oxia Planum observations, have been recently acquired by the PTAL project and will be included in the spectral library as well.

Data will be released and publicly available on the PTAL website database (Veneranda et al., 2018) before the term of the project (end of 2020). Several tools have been implemented on the website to help the user visualizing the full dataset. Samples will be available as well to the community for specific studies.

Declaration of competing interest

The authors declare that they have no known competing financial interests or personal relationships that could have appeared to influence the work reported in this paper.

CRediT authorship contribution statement

C. Lantz: Investigation, Visualization, Writing - original draft. **F. Poulet:** Supervision, Writing - original draft, Funding acquisition. **D. Loizeau:** Investigation, Writing - original draft. **L. Riu:** Resources. **C. Pilorget:** Resources. **J. Carter:** Resources. **H. Dypvik:** Resources. **F. Rull:** Funding acquisition, Data curation. **S.C. Werner:** Project administration, Funding acquisition.

Acknowledgements

This project is financed through the European Research Council in the H2020-COMPET-2015 programme (grant 687302). We warmly thank E.A. Cloutis and an anonymous referee for their constructive reviews.

Appendix A. Supplementary data

Supplementary data to this article can be found online at https://doi.org/10.1016/j.pss.2020.104989.

References

Adams, 1974. Visible and near-infrared diffuse reflectance spectra of pyroxenes as applied to remote sensing of solid objects in the solar system. J. Geophys. Res. 79, 4829–4836.
Agee, et al., 2013. Unique meteorite from early Amazonian Mars: water-rich basaltic breccia Northwest Africa 7034. Science 339, 780–785.
Armstrong, 1978. K-Ar dating: late Cenozoic McMurdo volcanic vroup and dry valley glacial history - Victoria Land - Antarctica. N. Z. J. Geol. Geophys. 21, 685–698.
Beegle, et al., 2017. SHERLOC on Mars 2020, P43G-01. AGU Fall Meeting.
Bibring, et al., 2006. Global mineralogical and aqueous Mars history derived from OMEGA/Mars Express data. Science 312, 400–404.
Bibring, et al., 2017. The MicrOmega investigation onboard ExoMars. Astrobiology 17, 621–626.
Bishop, et al., 2002. The influence of structural Fe, Al and Mg on the infrared OH bands in spectra of dioctahedral smectites. Clay Miner. 37, 607–616.
Bishop, et al., 2008. Reflectance and emission spectroscopy study of four groups of phyllosilicates: smectites, kaolinite-serpentines, chlorites and micas. Clay Miner. 43, 35–54.
Bultel, et al., 2015. Deep alteration between Hellas and Isidis basins. Icarus 260, 141–160.
Bultel, et al., 2019. Carbonates detection on Martian weathering profiles. J. Geophys. Res. 124, 989–1007.
Calvin, King, 1997. Spectral characteristics of iron bearing phyllosilicates: comparison to orgueil (CI1), murchison, and murray (CM2), meteorit. Planet. Sci. 32, 693–701.
Carrozzo, et al., 2017. Geology and mineralogy of the Auki Crater, Tyrrhena Terra, Mars: a possible post impact-induced hydrothermal system. Icarus 281, 228–239.

Carter, et al., 2013a. Hydrous minerals on Mars as seen by the CRISM and OMEGA imaging spectrometers: updated global view. J. Geophys. Res. 118, 831–858.
Carter, et al., 2013b. Automated processing of planetary hyperspectral datasets for the extraction of weak mineral signatures and applications to CRISM observations of hydrated silicates on Mars. Planet. Space Sci 76, 53–67.
Carter, et al., 2015. Widespread surface weathering on early Mars: a case for a warmer and wetter climate. Icarus 248, 373–382.
Carter, et al., 2016. Oxia Planum: a clay-laden landing site proposed for the ExoMars rover mission: aqueous mineralogy and alteration scenarios, 47th Lunar and Planetary Science Conference. LPI Contrib. 1903, 2064.
Cloutis, et al., 1986. Calibrations of phase abundance, composition, and particle size distribution for olivine-orthopyroxene mixtures from reflectance spectra. J. Geophys. Res. 91, 11641–11653.
Cloutis, Gaffey, 1991. Pyroxene spectroscopy revisited: spectral-compositional correlations and relationship to geothermometry. J. Geophys. Res. 96, 22809–22826.
Cloutis, et al., 2002. Spectral reflectance properties of zeolites and remote sensing implications. J. Geophys. Res. 107, 5067.
Cloutis, et al., 2006. Detection and discrimination of sulfate minerals using reflectance spectroscopy. Icarus 184, 121–157.
Crosta, et al., 2010. The first description and confirmation of the Vista Alegre impact structurein the Parana flood basalts of southern Brazil. Meteoritics Planet Sci. 45, 181–194.
Crosta, et al., 2012. Geology and impact features of Vargeão Dome - southern Brazil. Meteoritics Planet Sci. 47, 51–71.
De Sanctis, et al., 2017. Ma_MISS on ExoMars: mineralogical characterization of the Martian subsurface. Astrobiology 17, 612–620.
Dugdale, et al., 2020, Development of Oxia Planum simulant relevant to the ExoMars mission, 51st Lunar and Planetary Science Conference, LPI Contribution 2326, 2020, 2590
Dunning and Pedersen, 1988. U/Pb ages of ophiolites and arc-related plutons of the Norwegian Caledonides: implications for the development of Iapetus. Contrib. Mineral. Petrol. 98, 13–23.
Dypvik, et al., in prep, The Planetary Terrestrial Analogues Library (PTAL) - an Exclusive Lithological Selection of Possible Martian Earth Analogues.
Ehlmann, et al., 2008. Orbital identification of carbonate-bearing rocks on Mars. Science 322, 1828–1832.
Ehlmann, et al., 2009. Identification of hydrated silicate minerals on Mars using MRO-CRISM: geologic context near Nili Fossae and implications for aqueous alteration. J. Geophys. Res. 114, E00D08.
Ehlmann, Mustard, Murchie, 2010. Geologic setting of serpentine deposits on Mars. Geophys. Res. Lett. 37, L06201.
Ehlmann, et al., 2011. Subsurface water and clay mineral formation during the early history of Mars. Nature 479, 53–60.
Farmer, des Marais, 1999. Exploring for a record of ancient Martian life. J. Geophys. Res. 104, 26977–26996.
Fernández-Remolar, et al., 2004. The Tinto River, an extreme acidic environment under control of iron, as an analog of the Terra Meridiani hematite site of Mars. Planet. Space Sci. 52, 239–248.
Flahaut, et al., 2015. Embedded clays and sulfates in Meridiani Planum - Mars. Icarus 248, 269–288.
Flahaut, et al., 2019. The Italian Solfatara as an analog for Mars fumarolic alteration. Am. Mineral. 104, 1565–1577.
Furnes, Pedersen, Stillman, 1988. The Leka ophiolite complex - central Norwegian caledonides: field characteristics and geotectonic significance. J. Geol. Soc. London 145, 401–412.
Gendrin, et al., 2005. Sulfates in Martian layered terrains: the OMEGA/Mars Express view. Science 307, 1587–1591.
Gibson, Roger L., Reimold, Wolfe Uwe, 2008. In: Geology of the Vredefort Impact Structure: A Guide to Sites of Interest. South African Council for Geoscience, Pretoria.
Gohn, et al., 2008. Deep drilling into the Chesapeake Bay impact structure. Science 320, 1740–1745.
Goudge, et al., 2015. Assessing the mineralogy of the watershed and fan deposits of the Jezero crater paleolake system - Mars. J. Geophys. Res. Planets 120, 775–808.
Hicks, et al., 2014. Ferric saponite and serpentine in the nakhlite martian meteorites. Geochem. Cosmochim. Acta 136, 194–210.
Horgan, Christensen, 2013. Volcaniclastic paleosol sequences: an analog for reconstructing surface environments from clay-bearing layered deposits on Mars, conference on analog sites for Mars missions II: past, present and future missions to Mars. LPI Contrib. 1738, 4037.
Horgan, et al., 2014. Near-infrared spectra of ferrous mineral mixtures and methods for their identification in planetary surface spectra. Icarus 234, 132–154.
Hudson-Edwards, et al., 1999. Mineralogy and geochemistry of alluvium contaminated by metal mining in the Rio Tinto area - southwest Spain. Appl. Geochem. 14, 1015–1030.
Humayun, et al., 2013. Origin and age of the earliest Martian crust from meteorite NWA 7533. Nature 503, 513–516.
Hunt, Salisbury, 1971. Visible and near infrared spectra of minerals and rocks: II. Carbonates. Mod. Geol. 2, 23–30.
Iyer, et al., 2008. Serpentinization of the oceanic lithosphere and some geochemical consequences: constraints from the Leka Ophiolite Complex - Norway. Chem. Geol. 249, 66–90.
Kalleson, E, 2009. The Gardnos Structure: The Impactites, Sedimentary Deposits and Post-impact History. Faculty of Mathematics and Natural Sciences, University of Oslo.
King, Ridley, 1987. Relation of the spectroscopic reflectance of olivine to mineral chemistry and some remote sensing implications. J. Geophys. Res. 92, 11457–11469.
Klingelhöfer, et al., 2004. Jarosite and hematite at Meridiani Planum from Opportunity's mössbauer spectrometer. Science 306, 1740–1745.
Korablev, et al., 2017. Infrared spectrometer for ExoMars: a mast-mounted instrument for the rover. Astrobiology 17, 542–564.
Krzesińska, et al., 2019. Experimental constraints on the formation of vermiculitic, Fe,Mg-phyllosilicates on Mars with relevance to the aqueous history of Oxia Planum, Ninth international conference on Mars. LPI Contrib. 2089, 6216.
Krzesińska, et al., in prep.
Langer, Flörke, 1974. Near infrared absorption spectra (4000–9000 cm^{-1}) of opals and the role of "water" in these SiO 2 · nH 2 O minerals. Fortschr. Mineral. 52, 17–51.
Loizeau et al., submitted, Planetary terrestrial analogues library project: 2. Building of a laboratory facility for MicrOmega characterization, Planet. Space Sci..
Loizeau, et al., in prep, Planetary Terrestrial Analogues Library Project: 3. Characterization of Samples by the Near-Infrared Imaging Spectrometer MicrOmega.
Martinez-Frias, et al., 2004. The volcanism-related multistage hydrothermal system of El Jaroso (SE Spain): Implication for the exploration of Mars. Earth Planets Space 46, 5–8.
Michalski, et al., 2019. The geology and astrobiology of McLaughlin crater, Mars: an ancient lacustrine basin containing turbidites, mudstones, and serpentinites. J. Geophys. Res. Planets 124, 910–940.
Milliken, et al., 2008. Opaline silica in young deposits on Mars. Geology 36, 847–850.
Murchie, et al., 2009. A synthesis of Martian aqueous mineralogy after one Mars year of observations from the Mars Reconnaissance Orbiter. J. Geophys. Res. 114, E00D06.
Mustard, et al., 2007. Mineralogy of the Nili Fossae region with OMEGA/mex data: 1. Ancient impact melt in the Isidis basin and implications for the transition from the Noachian to hesperian. J. Geophys. Res. 112, E08S03.
Nash, Conel, 1974. Spectral reflectance systematics for mixtures of powdered hypersthene, labradorite, and ilmenite. J. Geophys. Res. 79, 1615–1621.
Neumann, et al., 1985. Compositional variations among gabbroic intrusions in the Oslo rift. Lithos 18, 35–59.
Poulet, et al., 2005. Phyllosilicates on Mars and implications for early martian climate. Nature 438, 623–627.
Poulet, et al., 2008b. Abundance of minerals in the phyllosilicate-rich units on Mars. Astron. Astrophys. 487, L41–L44.
Poulet, et al., 2009a. Key scientific questions and key investigations from the first international conference on Martian phyllosilicates. Astrobiology 9, 257–267.
Poulet, et al., 2009b. Quantitative compositional analysis of martian mafic regions using the MEx/OMEGA reflectance data: 2. Petrological implications. Icarus 201, 84–101.
Quantin-Nataf, et al., 2019. ExoMars at Oxia Planum: probing the aqueous-related Noachian environments, Ninth international conference on Mars. LPI Contrib. 2089, 6317.
Quantin-Nataf, et al., Submitted, Oxia Planum - the landing site for the 2020 ExoMars "Rosalind Franklin" rover mission: geological context and pre-landing interpretation, Astrobiology.
Rathbun, Squyres, 2002. Hydrothermal systems associated with Martian impact craters. Icarus 157–2, 362–372.
Retallack, et al., 2000. Eocene and oligocene paleosols of central Oregon. Geol. S. Am. S. 344. ISBN 9780813723440.
Rull, et al., 2017. The Raman laser spectrometer for the ExoMars rover mission to Mars. Astrobiology 17, 627–654.
Salisbury, et al., 1991. Infrared (2.1–25 Mm) Spectra of Minerals. John Hopkins Univ. Press, Baltimore, p. 267.
Schmincke, 1982. Volcanic and chemical evolution of the canary islands. In: von Rad, Hinz, Sarnthein, Seibold (Eds.), Geology of the Northwest African Continental Margin. Springer-Verlag, ISBN 9783642684111.
Schwenzer, Kring, 2013. Alteration minerals in impact-generated hydrothermal systems: exploring host rock variability. Icarus 226, 487–496.
Sherman, et al., 1982. Spectral characteristics of the iron oxides with application to the Martian bright region mineralogy. J. Geophys. Res. 87, 10169–10180.
Sigmarsson, Steinthorsson, 2007. Origin of Icelandic basalts: a review of their petrology and geochemistry. J. Geodyn. 43, 87–100.
Squyres, et al., 2008. Detection of silica-rich deposits on Mars. Science 320, 1063–1067.
Sun, Milliken, 2015. Ancient and recent clay formation on Mars as revealed from a global survey of hydrous minerals in crater central peaks. J. Geophys. Res. Planets 120, 2293–2332.
Sunshine, Pieters, 1993. Estimating modal abundances from the spectra of natural and laboratory pyroxene mixtures using the modified Gaussian model. J. Geophys. Res. 98, 9075–9087.
Sutter, et al., 2007. Terrestrial analogs for interpretation of infrared spectra from the Martian surface and subsurface: sulfate, nitrate, carbonate, and phyllosilicate-bearing Atacama Desert soils. J. Geophys. Res. 112, G04S10.
Troll, Carracedo, 2016. The Geology of the Canary Islands. Elsevier, ISBN 9780128096642.
Upton, et al., 2002. Picritic magmas and the Rum ultramafic complex - Scotland. Geol. Mag. 139, 437–452.
Veneranda, et al., 2018. PTAL database and website: developing a novel information system for the scientific exploitation of the planetary terrestrial analogues library, second international Mars sample return. LPI Contrib. 2071, 6069.
Veneranda, et al., 2019. Planetary terrestrial analogues library (PTAL) project: Raman data overview. J. Raman Spectrosc. 1–19. https://doi.org/10.1002/jrs.5652.
Viennet, et al., 2017. Dioctahedral phyllosilicates versus zeolites and carbonates versus zeolites competitions as constraints to understanding early Mars alteration conditions. J. Geophys. Res. Planets 122, 2328–2343.
Werner, et al., 2018. The planetary terrestrial analogues library (PTAL), second international Mars sample return. LPI Contrib. 2071, 6060.

Westall, et al., 2013. Habitability on Mars from a microbial point of view. Astrobiology 13, 887–897.
Wiens, et al., 2016. SuperCam remote sensing on the Mars 2020 rover: science goals and overview, 3rd international workshop on instrumentation for planetary mission. LPI Contrib. 1980, 4136.
Wiens, et al., 2017. The SuperCam remote Raman spectrometer for Mars 2020, 48th lunar and planetary science conference. LPI Contrib. 1964, 2600.
Wiseman, et al., 2010. Spectral and stratigraphic mapping of hydrated sulfate and phyllosilicate-bearing deposits in Northern sinus Meridiani - Mars. J. Geophys. Res. 115, E00D18.